Journal of Colloid and Interface Science 561 (2020) 11–22

Contents lists available at ScienceDirect

Journal of Colloid and Interface Science

journal homepage: www.elsevier.com/locate/jcis

Functionalized polymeric nanogels with pH-sensitive benzoic-imine cross-linkages designed as vehicles for indocyanine green delivery

Shu-Chiao Liao, Chih-Wei Ting, Wen-Hsuan Chiang *

Department of Chemical Engineering, National Chung Hsing University, Taichung 402, Taiwan

GRAPHICAL ABSTRACT

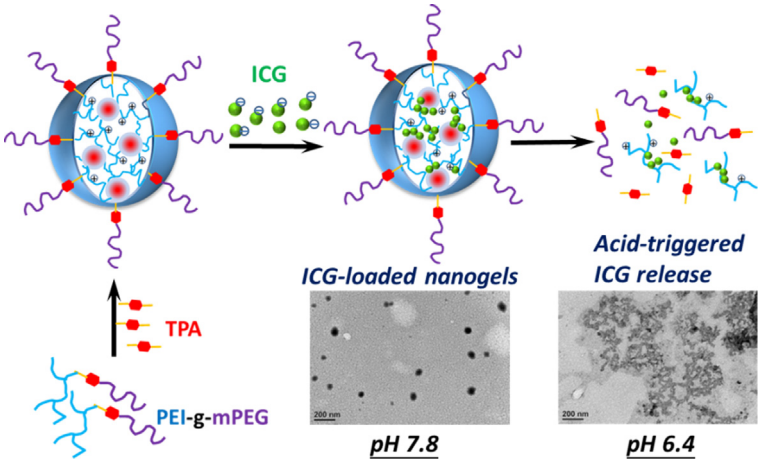

ARTICLE INFO

Article history:
Received 3 August 2019
Revised 3 November 2019
Accepted 27 November 2019
Available online 28 November 2019

Keywords:
Benzoic-imine bonds
Polymeric nanogels
Acid-triggered ICG release
Self-assembly
Hydrophobic microdomains

ABSTRACT

To expand clinical applications of indocyanine green (ICG) by overcoming its several drawbacks such as self-aggregation under physiological conditions, poor aqueous photostability, lack of target specificity and rapid renal elimination from the body, the functionalized polymeric nanogels with pH-responsive benzoic-imine cross-linkages employed as carriers for ICG delivery were developed by one-step cross-linking of the branched poly(ethylenimine)-g-methoxy poly(ethylene glycol) (PEI-g-mPEG) copolymer with hydrophobic terephthalaldehyde (TPA) molecules in aqueous solution of pH 7.4. Based on the findings of fluorescence, dynamic and static light scattering, and transmission electron microscopy measurements, the resulting polymeric nanogels exhibited a spherical structure comprising multiple hydrophobic benzoic-imine-rich microdomains covered by positively-charged PEI networks capable of holding large amounts of water, and hydrophilic mPEG segments. Moreover, the cross-linking of more TPA molecules with PEI-g-mPEG segments led to the formation of more microdomains inside the polymeric nanogels, thus making the colloidal structure more hydrophobic and compact. More importantly, through the electrostatic attraction of amphiphilic ICG molecules with protonated PEI segments as well as their hydrophobic association with microdomains upon π-π stacking, the ICG species can be efficiently encapsulated into the nanogels. Notably, the robust ICG-loaded nanogels showed several outstanding properties, including (1) significantly enhanced the photo-stability of ICG in phosphate buffer, (2) considerably retarded ICG leakage from nanogels at pH 7.8, (3) acid-triggered ICG release by the cleavage of benzoic-

* Corresponding author.
E-mail address: whchiang@dragon.nchu.edu.tw (W.-H. Chiang).

https://doi.org/10.1016/j.jcis.2019.11.109

imine bonds in response to pH reduction from 7.8 to 6.4. This work demonstrates that the pH-responsive polymeric nanogels have promising potential for tumor-targeted ICG delivery.

1. Introduction

Over the past two decades, varied stimuli-responsive polymeric nanogels utilized as drug delivery systems (DDS) have been extensively developed in view of their enhanced stability in blood circulation, outstanding biocompatibility, superior capability of carrying various pharmaceutically active ingredients ranging from small molecule drugs to biomacromolecules, and well-controlled drug release in response to environmental stimuli (e.g. pH, temperature, redox, glucose and light) [1–9]. Among these stimuli-responsive nanogels, the pH-sensitive polymeric nanogels designed as DDS have continuously captured substantial attention because the inherent pH difference between the blood/normal tissues (pH 7.4), tumor tissue (pH 7.0–6.5), intracellular acidic endosomes (pH 5.0–5.5) and lysosomes (pH 4.0–4.5) could be exploited for pH-triggered tumor-targeted drug delivery and intracellular drug liberation [10–12]. To date, despite the remarkable advances in the development of pH-responsive nanogels, several obstacles including non-biodegradability, incomplete drug release and intricate preparation procedure involving the core/shell cross-linking of preformed polymeric micelles still largely limit their clinical applications [13,14].

In order to conquer the above issues, varied acid-labile moieties such as acetal, orthoester, hydrazone and ketal bonds have been combined with the hydrophilic polymer chains in simple manner for fabrication of pH-responsive nanogels [2,15–20]. For example, Song and co-workers developed the hyaluronic acid (HA)-based nanogels with ketal-containing cross-linkers by free radical polymerization of one-pot process [2]. Through the acid-activated fast degradation of ketal linkages to destroy nanogels, a burst and substantial release of doxorubicin (DOX) loaded within nanogels was achieved under acidic condition. As a result, the pH-responsive DOX-loaded nanogels showed outstanding antitumor efficacy on H22 tumor-bearing mice. As reported by Tang's group, [20] the acid-degradable nanogels were obtained upon the cross-linking of carboxymethyl chitosan (CMCS) with cyclic ortho ester-containing cross-linker by a simple emulsion-solvent evaporation technique. The resulting nanogels exhibited pH-triggered size change, degradation and drug release by the hydrolysis of acid-labile ortho ester bonds under weak acidic condition, thus effectively delivering payloads into tumor-like multicellular spheroids. However, for these nanogels consisting of the hydrophilic polymers and cross-linkers, their application for the transport of poorly water-soluble drugs faces challenges due to the lack of hydrophobic domains used frequently as binding sites of the lipophilic and amphiphilic therapeutic agents. In order to selectively deliver hydrophobic drugs to tumor region by using the pH-sensitive nanogels, Lee's group adopted one-step approach to prepare pH-responsive polymeric nanogels constructed from the cross-linking of hydrophilic methoxy poly(ethylene glycol)-*b*-poly[N-[N-(2-aminoethyl)-2-aminoethyl]-l-glutamate] (mPEG-*b*-PNLG) with hydrophobic terephthalaldehyde (TPA) [13]. By the formation of acid-degradable benzoic-imine bonds [10,13], the resulting hydrophobic PNLG/TPA core inside nanogels was employed as a reservoir of hydrophobic DOX in free base form. The DOX-carrying nanogels underwent acid-triggered disassembly due to cleavage of benzoic-imine leakages to achieve rapid and efficient drug release, whereas maintained stable colloidal structure at normal physiological pH.

Indocyanine green (ICG), an amphiphilic tricarbocyanine dye, has been approved by the United States Food and Drug Administration for clinical use of ophthalmology and cardiac imaging [21,22]. Also it can convert near-infrared (NIR) light to generate heat and reactive oxygen species (ROS) for cancer photothermal and photodynamic therapy [21,22]. Recently, for expand clinical applications of ICG by overcoming its several drawbacks such as self-aggregation under physiological conditions, lack of target specificity and rapid renal elimination from the body, various nanoparticles such as liposomes, polymeric micelles, polymersomes and nanogels have been created as carriers for ICG delivery [23,24]. However, for most of the aforementioned pH-responsive nanogels, due to their innate hydrophilicity and lack of hydrophobic domains, the effective and stable loading of ICG are largely limited. To develop the pH-responsive polymeric nanogels capable of realizing sufficient ICG loading and well-controlled ICG release, in this work, the benzoic-imine-bearing poly(ethylenimine) (PEI)-*g*-mPEG copolymer was synthesized and further covalently cross-linked with hydrophobic TPA molecules upon the formation of extra acid-labile benzoic-imine cross-linkages between primary amine of PEI and aldehyde of TPA (Scheme 1). Moreover, the structural characteristics of polymeric nanogels formed at different TPA concentrations and their pH-responsive properties were investigated by dynamic/static light scattering (DLS/SLS) technique, transmission electron microscopy (TEM), fluorescence and zeta potential measurements. Through the hydrophobic association of ICG molecules with the positively-charged and benzoic-imine-containing polymeric nanogels upon the combined electrostatic interaction and π-π stacking, the ICG-carrying polymeric nanogels were attained. Furthermore, the optical and colloidal stability of ICG-encapsulated nanogels and their cargo release profiles in response to pH change were further studied to evaluate the potential of ICG-loaded polymeric nanogels for the application of cancer diagnosis and treatment.

2. Experimental section

2.1. Materials

ICG (95.4%) was purchased from Chem-Impex (USA). mPEG (M.W. = 1.9 kDa, 98%), branched PEI (M.W. = 1.8 kDa, 99%), TPA (98%) and pyrene (98%) were acquired from Alfa Aesar (USA). *p*-formylbenzoic acid (95%), *N*-hydroxysuccinimide (NHS, 98%), N,N′-dicyclohexylcarbodiimide (DCC, 99%), 4-dimethylaminopyridine (DMAP, 98%) and D_2O (99.9 atom % D) were purchased from Sigma-Aldrich (USA). Deionized water was produced from Milli-Q Synthesis (18 MΩ, Millipore). All other chemicals were reagent grade and used as received.

2.2. Synthesis of methoxy poly(ethylene glycol) benzaldehyde (mPEG-CHO)

The mPEG-CHO utilized in the work was synthesized by the DCC/DMAP-mediated esterification of mPEG with *p*-formylbenzoic acid as illustrated in Scheme 2. *p*-formylbenzoic acid (4.73 g, 3.15×10^{-2} mol), mPEG (6 g, 3.15×10^{-3} mol), DCC (6.52 g, 3.15×10^{-2} mol) and DMAP (0.96 g, 7.89×10^{-3} mol) were dissolved in dry DCM (100 mL). The reaction was performed under stirring at room temperature for 24 h. After being filtrated to

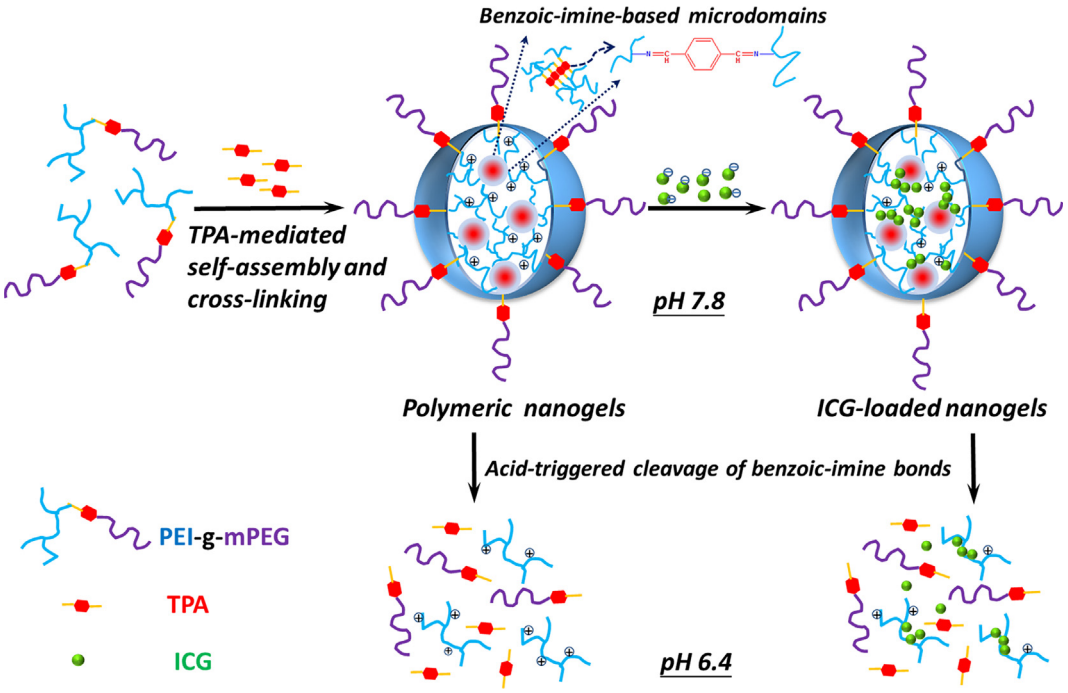

Scheme 1. Illustration of development of pH-responsive ICG-loaded polymeric nanogels for controlled ICG release.

remove dicyclohexylcarbodiurea, the solution was concentrated by a rotary evaporator. Subsequently, the product was collected by precipitation from cold diethyl ether and washed with isopropanol. The product was dried under vacuum at room temperature overnight.

2.3. Synthesis of benzoic-imine-containing PEI-g-mPEG

The synthesis of PEI-g-mPEG based on Schiff base reaction of mPEG-CHO and branched PEI is illustrated in Scheme 2. Briefly, PEI (100 mg), mPEG-CHO (20 mg) and DMAP (10 mg) were directly dissolved in DMSO (2.0 mL). The solution was stirred at room temperature for 72 h and then dialyzed (Cellu Sep MWCO 3500) against 0.01 M pH 7.4 phosphate buffer at 4 °C to remove DMSO. Finally, the product was collected by lyopholization.

2.4. Characterization of mPEG-CHO and benzoic-imine-containing PEI-g-mPEG

The chemical structures of mPEG-CHO and PEI-g-mPEG were analysed by Fourier transform infrared (FT-IR) spectroscopy (FT-720, HORIBA, Japan) using KBr pellet, and proton nuclear magnetic resonance (^{1}H NMR) spectroscopy (Agilent DD2 600 MHz NMR spectrometer) using D_2O as the solvent. Moreover, the molecular weight (M_w) and polydispersity index (PDI) of mPEG-CHO and PEI-g-mPEG were measured by gel permeation chromatography (GPC) (Agilent 1100, PL aqueous 30 column, separation range 100–30,000 Da), calibrated with PEG standards of known molecular weights with narrow molecular weight distributions, using pH 7.4 phosphate buffer as the eluent at a flow rate of 0.3 mL/min and 25 °C under refractive index detector (Agilent 1100).

2.5. Preparation of pristine polymeric nanogels and ICG-loaded polymeric nanogels

First, PEI-g-mPEG (2.0 mg) was dissolved in pH 7.4 phosphate buffer (1.8 mL). Subsequently, the DMSO solution containing TPA with different concentrations (0.2 mL) was added dropwise into the aqueous copolymer solution under stirring. The mixture was mildly stirred at room temperature for 24 h and then dialyzed (Cellu Sep MWCO 12000 ~ 14000) with pH 7.8 phosphate buffer at 4 °C to remove DMSO. For preparation of ICG-loaded polymeric nanogels, the DMSO solution containing ICG (2.0 mg/mL, 0.05 mL) was slowly dropped into the aqueous nanogel suspension (pH 7.4) under stirring and stirred at room temperature for 1 h. Through the dialysis (Cellu Sep MWCO 12,000–14,000) of the ICG-containing suspension against 0.01 M pH 7.8 phosphate buffer at 4 °C for 24 h to eliminate unloaded ICG and DMSO, the purified ICG-loaded nanogels were attained.

2.6. Structural characterization

The mean hydrodynamic particle diameter (D_h) and particle size distribution of pristine nanogels and ICG-loaded nanogels in aqueous solutions were measured by a Brookhaven BI-200SM goniometer equipped with a BI-9000 AT digital correlator using a solid-state laser (35 mW, λ = 637 nm) detected at a scattering angle of 90°. The data presented herein represent an average of at least triplicate measurements. Also, the angular dependence of the auto-correlation functions was evaluated with the above instrument. Correlation functions were analyzed by the cumulant method at different angles. To explore the morphology of pristine polymeric nanogels, the ratio of the root-mean-square radius of gyration (R_g) to the mean hydrodynamic radius (R_h) of nanogels was attained by dynamic and static light scattering (DLS/SLS) measurements using the same instrument. For the quantitative determination of R_g of polymeric nanogels, the Berry plot of the scattering intensity ($I_{ex}^{-1/2}$) versus the square of the scattering vector (q^2) was acquired by the angle-dependent measurements of the light scattering intensity. On the other hand, the zeta potential of polymeric nanogels in aqueous solutions was determined by a Nanobrook 90Plus PALS (Brookhaven, USA).

In order to quantify ICG loaded within nanogels, a preset volume of the purified drug-loaded nanogel solution was freeze-

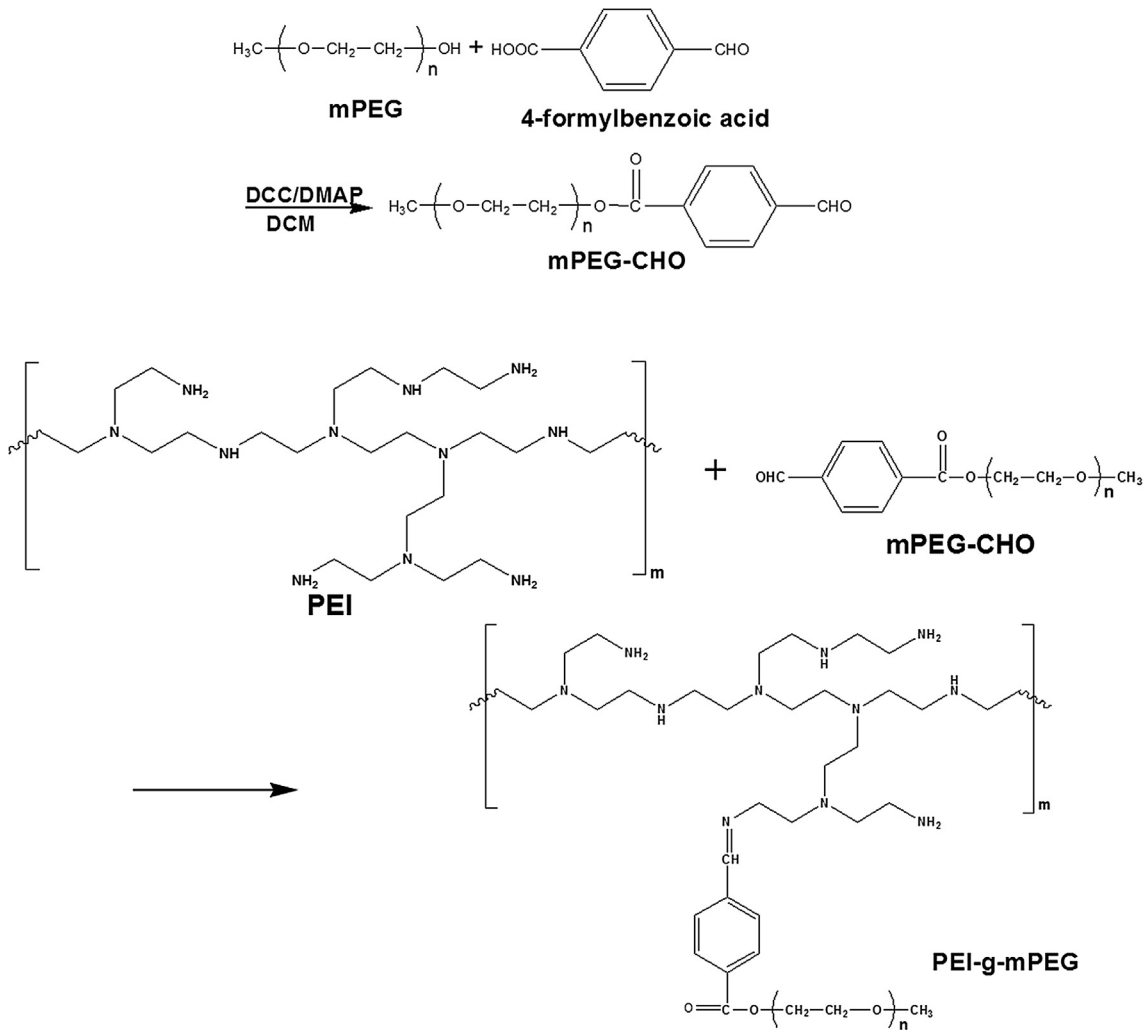

Scheme 2. Synthetic route of the mPEG-CHO and benzoic-imine-containing PEI-g-mPEG copolymer.

dried and then re-dispersed into pH 5.0 aqueous solution to destroy nanogel structure for drug extraction. The amount of ICG encapsulated was determined using a UV/Vis spectrophotometer (U2900, Hitachi, Japan). The absorbance of ICG at 719 nm was recorded. The calibration curve used for drug loading analysis was established by absorbance of ICG with varying concentrations in aqueous solution of pH 5.0. Drug loading efficiency (DLE) and drug loading content (DLC) were estimated by the following formulas

$$\text{DLE}\ (\%) = (\text{weight of loaded ICG/weight of ICG in feed}) \times 100\%.$$

$$\text{DLC}\ (\%) = (\text{weight of loaded ICG/total weight of the purified ICG} - \text{loaded nanogel solution after lyophilization}) \times 100\%.$$

2.7. Fluorescence measurements

Pyrene, a nonpolar probe, was used in fluorescence characterization. Aliquots (20.0 μL) of pyrene in acetone (3.0×10^{-5} M) were evaporated in vials, followed by addition of the aqueous nanogel suspensions (1.0 mL) at the predetermined pH. The resulting sample was kept at 4 °C for 12 h to obtain the nanogel dispersions with a constant pyrene concentration of ca 6.0×10^{-7} M. The fluorescence emission spectra of pyrene in the nanogel dispersions were attained using a Hitachi F-2700 fluorescence spectrometer. The excitation was performed at 336 nm and the emission was recorded in the range from 350 to 500 nm. The fluorescence intensity ratios (I_3/I_1) of the third vibrionic band at 385.5 nm to the first at 373.5 nm of pyrene in the nanogel solutions were obtained.

2.8. Transmission electron microscopy (TEM) examination

TEM images of pristine polymeric nanogels and ICG-loaded nanogels were acquired from a JEOL JEM-1400 CXII microscope operating at an accelerating voltage of 120 kV. Samples were prepared by placing a few drops of the nanogel solution on a 300-mesh copper grid covered with carbon and then negatively stained with uranyl acetate (2.0 wt%) for 30 s and dried at 25 °C for 2 days before TEM observation.

2.9. In vitro ICG release profiles

For ICG release study, the ICG-loaded nanogel solutions (3.0 mL) was dialyzed (Cellu Sep MWCO 12,000 ~ 14,000) against phosphate buffer (pH 7.8) and acetate buffer (pH 6.4) (40 mL), respectively, under gentle shake (100 rpm) at 37 °C. The internal sample solution was withdrawn periodically for determination of maximum ICG absorbance. The sample solution was placed back into the dial-

ysis tube after each measurement. The cumulative ICG release (%) was calculated by the formula:

$$\text{Cumulative ICG release}(\%) = ((\text{Initial ICG absorbance} - \text{ICG absorbance at different time points})/\text{initial ICG absorbance}) \times 100\%.$$

3. Results and discussion

3.1. Synthesis and characterization of mPEG-CHO

The mPEG-CHO employed in this work was attained by the DCC/DMAP-mediated esterification of mPEG with *p*-formylbenzoic acid [25]. As shown in Fig. 1, the FT-IR spectrum of *p*-formylbenzoic acid exhibited the characteristic absorption band at 1691 cm^{-1} from C=O stretching vibration of aldehyde and carboxylic acid groups. After *p*-formylbenzoic acid was conjugated with mPEG, the FT-IR spectrum of mPEG-CHO displayed the characteristic absorption bands at 1110 cm^{-1} and 2881 cm^{-1} for C—O and C—H stretching vibration of mPEG, respectively, and at 1641 and 1700 cm^{-1} for C=O stretching vibration of ester and aldehyde groups, respectively, which were absent in mPEG. This indicates the successful conjugation of mPEG and *p*-formylbenzoic acid. Moreover, as shown in the ^1H NMR spectrum of mPEG-CHO in D_2O (Fig. 2a), based on the signal integral ratio of the aldehyde proton of *p*-formylbenzoic acid at δ 10.1 ppm and the methyl protons of mPEG at δ 3.4 ppm, the coupling efficiency was estimated to be ca. 95%.

3.2. Synthesis and characterization of benzoic-imine-containing PEI-g-mPEG

The PEI-g-mPEG with benzoic-imine linkages was prepared by Schiff base reaction between primary amine and aldehyde groups from branched PEI and mPEG-CHO segments, respectively. As presented in the FT-IR spectrum of PEI-g-mPEG (Fig. 1e), in addition to a complete disappearance of feature band of C=O stretching vibration of aldehyde group at 1700 cm^{-1}, the characteristic absorption bands at 1110 and 3300–3500 cm^{-1} ascribed to C—O stretching vibration of mPEG-CHO and N—H stretching vibration of PEI, respectively, were observed. Also, the ^1H NMR spectrum of PEI-g-mPEG (Fig. 2b) showed the disappearance of the proton signal of aldehyde group at δ 10.1 ppm from mPEG-CHO and the appearance

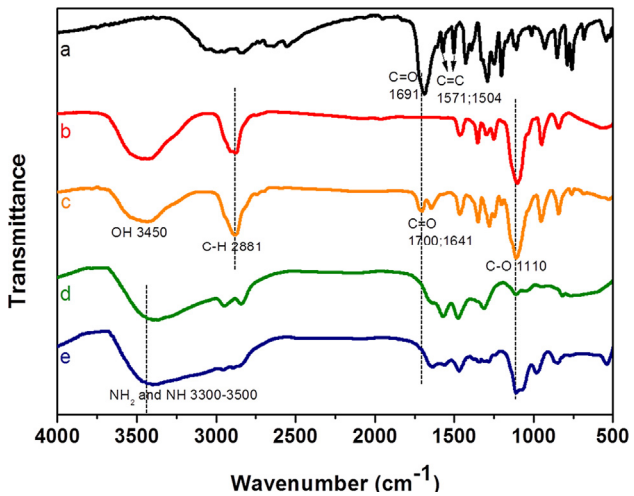

Fig. 1. FT-IR spectra of (a) 4-formylbenzoic acid, (b) mPEG, (c) mPEG-CHO, (d) PEI and (e) PEI-g-mPEG.

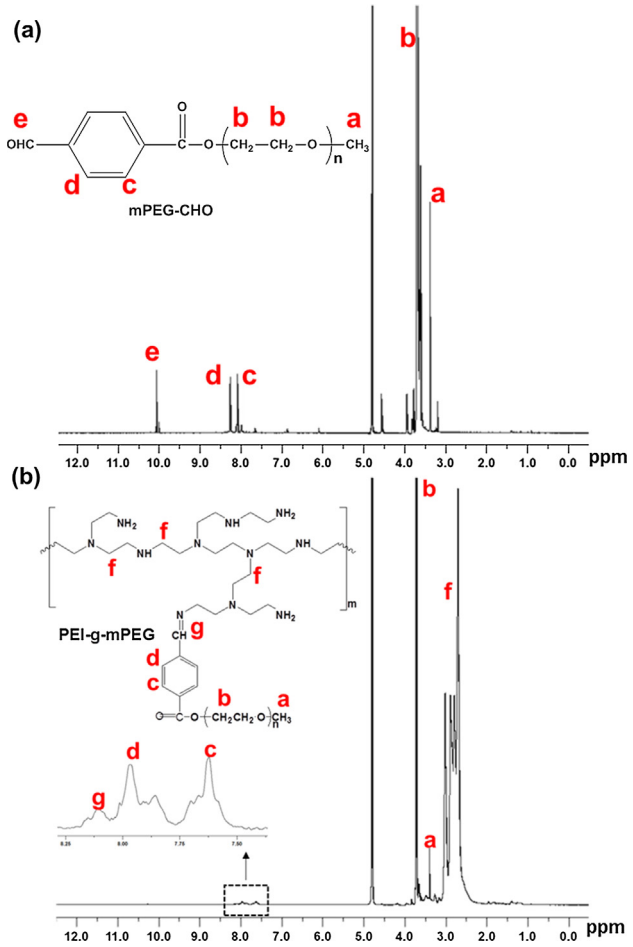

Fig. 2. ^1H NMR spectra of (a) mPEG-CHO and (b) PEI-g-mPEG in D_2O.

of HC = N proton signal of benzoic-imine group at δ 8.2 ppm. According to the signal integral ratio of the methyl protons of mPEG at δ 3.4 ppm and the ethylenimine protons of PEI at δ 2.6 ppm, 1.2 mol % of EI units in PEI was conjugated with mPEG-CHO segments. The molecular weight of PEI-g-mPEG was calculated to be 2750 g/mol by ^1H NMR analysis. As revealed in Fig. S1, the GPC curve of the resultant PEI-g-mPEG shifts toward a higher molecular weight compared to that of mPEG-CHO and branched PEI. The molecular weight of PEI-g-mPEG determined by GPC is ca. 2560 g/mol, which agrees with the result of ^1H NMR analysis. These findings clearly illustrate the successful conjugation between PEI and mPEG-CHO segments upon the formation of benzoic-imine bonds.

In order to attain the polymeric nanogels with different CHO/NH_2 ratios by adjusting the concentration of PEI-g-mPEG and TPA in feed, the PEI content of PEI-g-mPEG was calculated to be ca. 65 wt% by the formula:

$$Weight\ fraction(\%PEI) = \frac{100 \times M.W.EI}{(Grafting\ ratio \times M.W.PEG) + (100 \times M.W.EI)} \times 100\%.$$

Based on the obtained PEI content of PEI-g-mPEG, the NH_2 content of PEI-g-mPEG of 1.0 mg was calculated to be ca. 4.8 mmol.

3.3. Development and characterization of PEI-g-mPEG/TPA nanogels

Due to the formation of acid-degradable benzoic-imine cross-linkages, the colloidal structure was developed at pH 7.4 by the

covalent cross-linking of the PEI-g-mPEG segments with TPA molecules of different concentrations. In the absence of TPA molecules (CHO/NH_2 ratio = 0), the PEI-g-mPEG copolymer solution (1.0 mg/mL) exhibited a very low light scattering intensity and nearly transparent state (Fig. 3a and b), reflecting that the graft copolymer exists in highly hydrated and unimolecular form. Notably, as the CHO/NH_2 ratio in feed was increased from 0.4 to 1.6, in addition to the considerable reduction of mean hydrodynamic diameter (D_h) of the resulting colloidal particles from 2000 nm to 158 nm, an appreciable rise in the light scattering intensity of polymeric colloidal solutions was observed in DLS characterization (Fig. 3a). Corresponding to the DLS data, the phase transition of PEI-g-mPEG/TPA mixture solutions from clear to opaque state with increasing CHO/NH_2 ratios as shown in Fig. 3b is indicative of development of polymeric colloidal structure. It is worthy to note that the nanogels formed at a CHO/NH_2 ratio of 2.3 exhibit a smaller size (ca. 120 nm) and relatively narrow particle size distribution (PDI 0.12) compared to those fabricated at CHO/NH_2 ratios of 0.4 and 1.2 (Fig. 3c). In addition, the polymeric nanogels (CHO/NH_2 ratio = 2.3) have a nearly neutral surface as reflected by the slightly positive values (+4.3 mV) of their zeta potential. With the CHO/NH_2 ratio being further elevated from 2.3 to 3.9, the visibly enlarged particle size and size distribution of the polymeric nanogels were attained by both DLS and TEM measurements (Fig. 3c and Fig. S2), implying the occurrence of nanogel agglomeration. Herein, the formation of polymeric colloidal structure could involve the following processes. At first, the hydrophilic PEI-g-mPEG segments after being conjugated with hydrophobic TPA molecules via benzoic-imine bonds could transform to the amphiphilic property. Subsequently, the π-π stacking-elicited self-assembly of amphiphilic TPA-conjugated PEI-g-mPEG segments and their covalent cross-linking generate the colloidal particles (Scheme 1). According to the DLS results, it was assumed that the cross-linking of PEI-g-mPEG segments with a small number of TPA molecules (CHO/NH_2 = 0.4) could tend to form quite loose and large colloidal structure due to the lack of adequate benzoic-imine cross-linkages. By increasing TPA concentration, the development of more benzoic-imine cross-linkages within the polymeric nanogels could endow the resulting nanogels with relatively hydrophobic and robust structure. As a consequence, the polymeric nanogels formed at a CHO/NH_2 ratio of 2.3 suffering large-volume dilutions with phosphate buffer maintained virtually unvaried particle size (Fig. 3d). On the other hand, it was found that the cross-linking of PEI segments instead of PEI-g-mPEG with TPA species at a CHO/NH_2 ratio of 2.3 was apt to produce quite huge colloidal particles (ca. 413 nm) with positively-charged surface (+12.7 mV) as presented in DLS data (Fig. S3). Also a substantial aggregation of PEI/TPA-based colloidal particles was observed in TEM images (Fig. S4). Such a difference in the particle size and zeta potential between the aforementioned colloidal particles clearly elucidates that, during self-assembly and cross-linking of PEI-g-mPEG copolymer chains and TPA molecules, the hydrophilic mPEG grafts have high tendency of residing at the surfaces of polymeric nanogels to effectively not only prevent colloidal particles from aggregation and inter-particle cross-linking upon their steric repulsion effect, but also shield the surface positive charges.

In order to get insight into the effects of CHO/NH_2 ratios on the colloidal structure, fluorescence characterization of the polymeric colloidal solutions at pH 7.8, using pyrene as the probe, was conducted. Because the nonpolar pyrene molecules tend to diffuse into

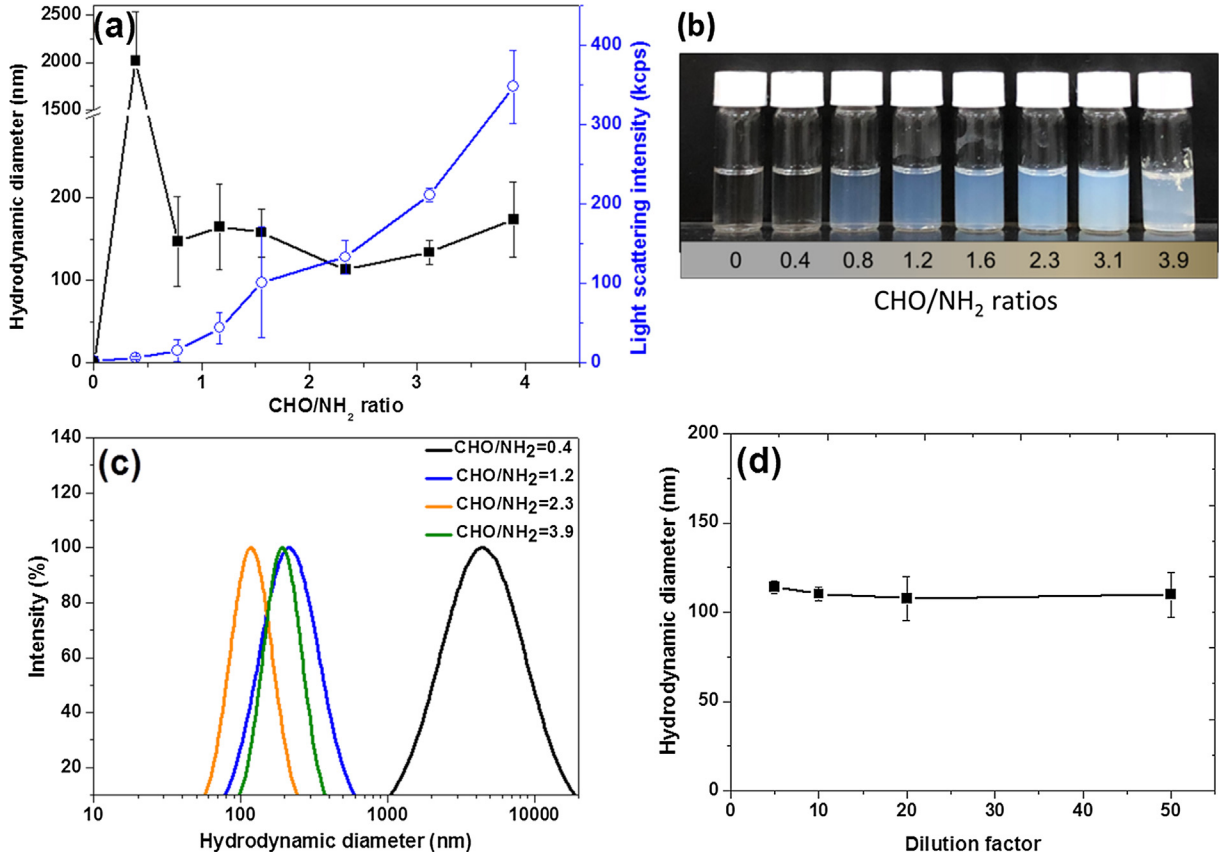

Fig. 3. (a) Hydrodynamic diameters and light scattering intensity of polymeric colloidal particles with various CHO/NH_2 ratios in aqueous solutions of pH 7.8. (b) Photographs of aqueous solutions of polymeric colloidal particles with various CHO/NH_2 ratios. (c) DLS size distribution profiles of polymeric colloidal particles with various CHO/NH_2 ratios in aqueous solutions of pH 7.8. (d) Hydrodynamic diameters of polymeric nanogels (CHO/NH_2 ratio = 2.3) after phosphate buffer dilution.

the hydrophobic domains of aqueous polymer solutions, the fluorescence intensity ratio (I_3/I_1) of pyrene can reflect the hydrophobicity nature of the polymeric assemblies [26–28]. As shown in Fig. 4, in the absence of TPA molecules, the I_3/I_1 value of pyrene in aqueous solution of PEI-g-mPEG determined to be ca. 0.59 comparable to that of pyrene alone in water demonstrates that the PEI-g-mPEG segments existed in the highly hydrated unimer state. Notably, the I_3/I_1 value of pyrene in polymeric colloidal solutions was significantly increased from 0.63 to 0.92 with the CHO/NH_2 ratio being adjusted from 0.4 to 3.9. This strongly verifies our postulation that the addition of more TPA molecules to cross-link PEI-g-mPEG segments enables the formation of more benzoic-imine linkages inside the polymeric nanogels, thus making the colloidal structure more hydrophobic.

For the purpose of investigating the geometric characteristics of polymeric nanogels, the variable angle DLS and SLS measurements were executed in combination with TEM observation. In the angle-dependent DLS measurement of polymeric nanogels with CHO/NH_2 ratios of 2.3 and 1.2 dispersed in aqueous solution (pH 7.8), a linear relationship between the relaxation frequency (Γ) and the square of the scattering vector (q^2) was attained as presented in Fig. 5a and b. This suggests that these polymeric nanogels in aqueous solutions display a spherical shape [4,29,30]. Also the R_g value of polymeric nanogels with CHO/NH_2 ratios of 2.3 and 1.2 was determined to be 65.7 nm and 109.3 nm, respectively, from the Berry plot of $I_{ex}^{-1/2}$ versus q^2 by angle-dependent SLS analysis (Fig. 5a and b). Considering that R_g is intimately related to the mean distance of individual groups that fabricate the target assembly to its mass center, whereas R_h is the radius of a theoretical solid sphere that diffuses with the same speed as the target under measurement [31], the R_g/R_h ratio is sensitive to the topology of polymeric assemblies [32–34]. Notably, for the polymeric nanogels with CHO/NH_2 ratios of 2.3 and 1.2, the obtained R_g/R_h values of ca.1.09 and 1.29, which are close to the R_g/R_h values (0.9–1.3) of various cationic nanogels reported elsewhere [32], strongly demonstrates that the gel-like spheres can be generated by the cross-linking of PEI-g-mPEG segments with TPA molecules, but lack the single hydrophobic core (note that a R_g/R_h value of 0.77 signifies the construction of solid sphere-like nanoparticles). Distinct from the cross-linking of mPEG-*b*-PNLG and TPA to form polymeric nanogels with single hydrophobic PNLG/TPA-constituted core structure as reported by Lee's group [13], in this work, due to the inter-chain electrostatic repulsion force of the positively-charged PEI-g-mPEG segments as well as their branched shape-induced steric hindrance, during cross-linking of PEI-g-mPEG and TPA, the resulting benzoic-imine linkages undergoing π-π stacking inclined to form multiple hydrophobic microdomains instead of single hydrophobic core (Scheme 1). Moreover, the lower R_g/R_h ratio (ca. 1.09) of polymeric nanogels with a CHO/NH_2 ratio of 2.3 than that (ca. 1.29) of the polymeric nanogels with a CHO/NH_2 ratio of 1.2 reflects that the colloidal structure of the former is constructed by tight cross-linking of PEI-g-mPEG segments with numerous hydrophobic microdomains. A similar finding regarding the effects of cross-linking degree of polymeric nanogels on their R_g/R_h ratios was also reported elsewhere [34].

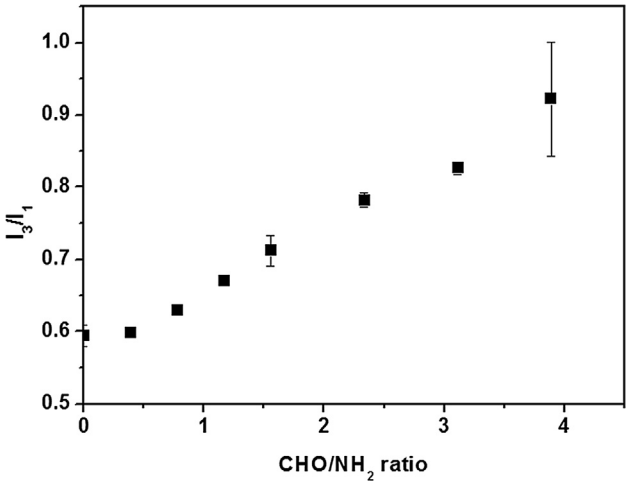

Fig. 4. Fluorescence intensity ratio (I_3/I_1) of pyrene in aqueous solutions of polymeric colloidal particles with different CHO/NH_2 ratios.

On the other hand, the TEM images in Fig. 5c showed that the polymeric nanogels (CHO/NH_2 ratio = 2.3) were well-dispersed and spherical. Similar TEM images of the spherical polymeric nanogels with negative staining were also observed elsewhere [35–37]. By contrast, as revealed in Fig. 5d, the polymeric nanogels (CHO/NH_2 ratio = 1.2) showed an non-spherical form. Such a difference in the morphology of dried nanogels illustrates that the sufficient cross-linking of PEI-g-mPEG segments with TPA molecules (CHO/NH_2 ratio = 2.3) renders the nanogels with a robust structure to resist the deformation during the removal of water molecules from the nanogels for TEM sample preparation. Furthermore, due to the transition of nanogels from swollen state (DLS) to dried state (TEM), the particle sizes of polymeric nanogels determined by DLS are somewhat larger than those observed by TEM [38,39]. Based on the above data, the PEI-g-mPEG/TPA polymeric nanogels attained at a CHO/NH_2 ratio of 2.3 showed the robust colloidal structure, relatively small particle size and narrow size distribution, thereby being employed for subsequent experiments.

In view of the polymeric nanogels comprising acid-labile benzoic-imine cross-linkages, they are expected capable of showing pH-responsive property. As presented in Fig. 6a, the prominent phase transition of nanogel solutions from opaque to transparent state was observed with the solution pH being adjusted from 7.8 to 6.4. Moreover, when the medium pH was lowered from 7.8 to 6.4, the particle size of polymeric nanogels was markedly enlarged from 120 to 520 nm at 4 h post pH stimulation and then significantly decreased to below 5 nm at 24 h post pH stimulation (Fig. 6b), indicating swollen and disintegration of the nanogels under weak acidic condition. In agreement with the DLS characterization, very few aggregates with particle size less than 10 nm were also observed in TEM images of polymeric nanogels at pH 6.4 (Fig. 6c). Furthermore, Fig. 6d showed a remarkable decline in I_3/I_1 ratio of pyrene in the nanogel solutions from 0.78 to 0.59 in response to pH reduction. These results reveal that the stable nanogels undergoing acid-triggered extensive cleavage of benzoic-imine bonds could be completely disassociated into highly hydrated polymeric segments such as PEI and mPEG-CHO (Scheme 1). On the other hand, with the medium pH being adjusted from pH 7.8 to 6.4, the increased protonation of amine groups of PEI segments as reported elsewhere [40] and the destruction of polymeric nanogels led to a considerable change of the zeta potential from +4.3 mV (pH 7.8) to +41.0 mV (pH 6.4).

3.4. ICG loading and in vitro release

In this work, it was expected that the amphiphilic sulfonate group-containing ICG molecules could be stably enclosed in the nanogels by forming hydrophobic ionic complexes with positively-charged PEI segments via electrostatic interaction and associating with hydrophobic benzoic-imine-rich microdomains upon π-π aromatic stacking. In order to verify the feasibility of the concepts, ICG in DMSO was added dropwise to phosphate buffer (pH 7.8) containing PEI segments. Remarkably, compared to well dispersion of ICG alone in aqueous solution over 1 h, substantial green precipitates were instantly generated at the bottom of

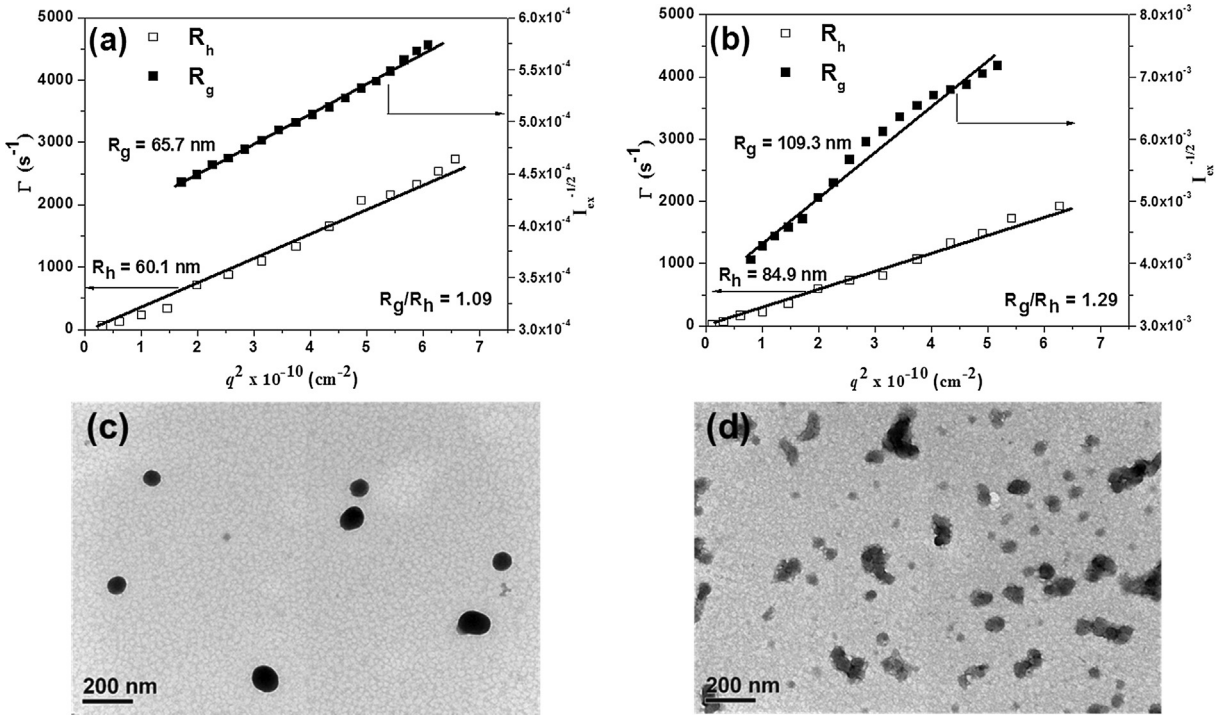

Fig. 5. Berry plot [29] for R_g and angle-dependent correlation function [30] for R_h of polymeric nanogels with CHO/NH_2 ratios of (a) 2.3 and (b) 1.2. TEM images of polymeric nanogels with CHO/NH_2 ratios of (c) 2.3 and (d) 1.2.

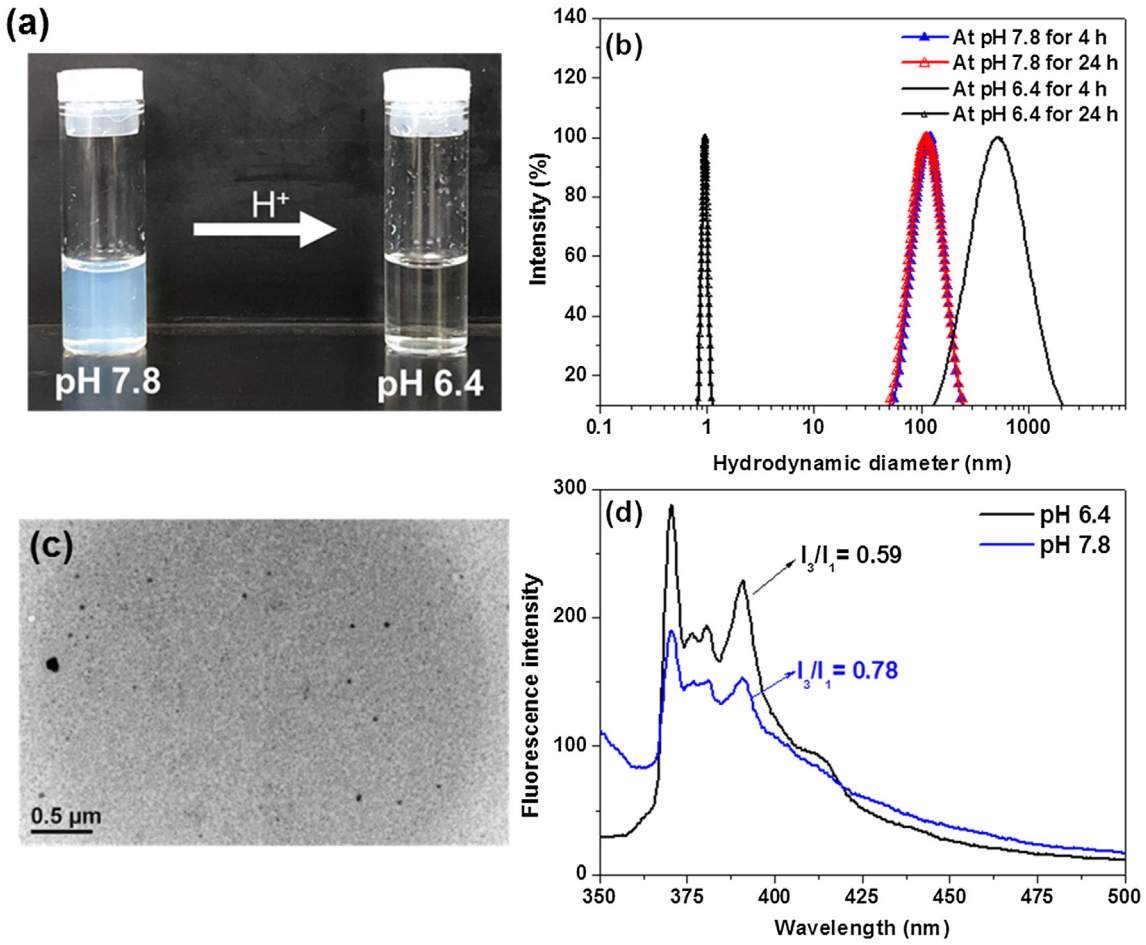

Fig. 6. (a) Photograph of polymeric nanogel (CHO/NH_2 = 2.3) solutions at pH 7.8 and 6.4. (b) DLS size distribution profiles of polymeric nanogels in aqueous solutions at pH 7.8 and 6.4. (c) TEM images of polymeric nanogels at pH 6.4. (d) Fluorescence spectra of pyrene in polymeric nanogel solutions at pH 7.8 and 6.4.

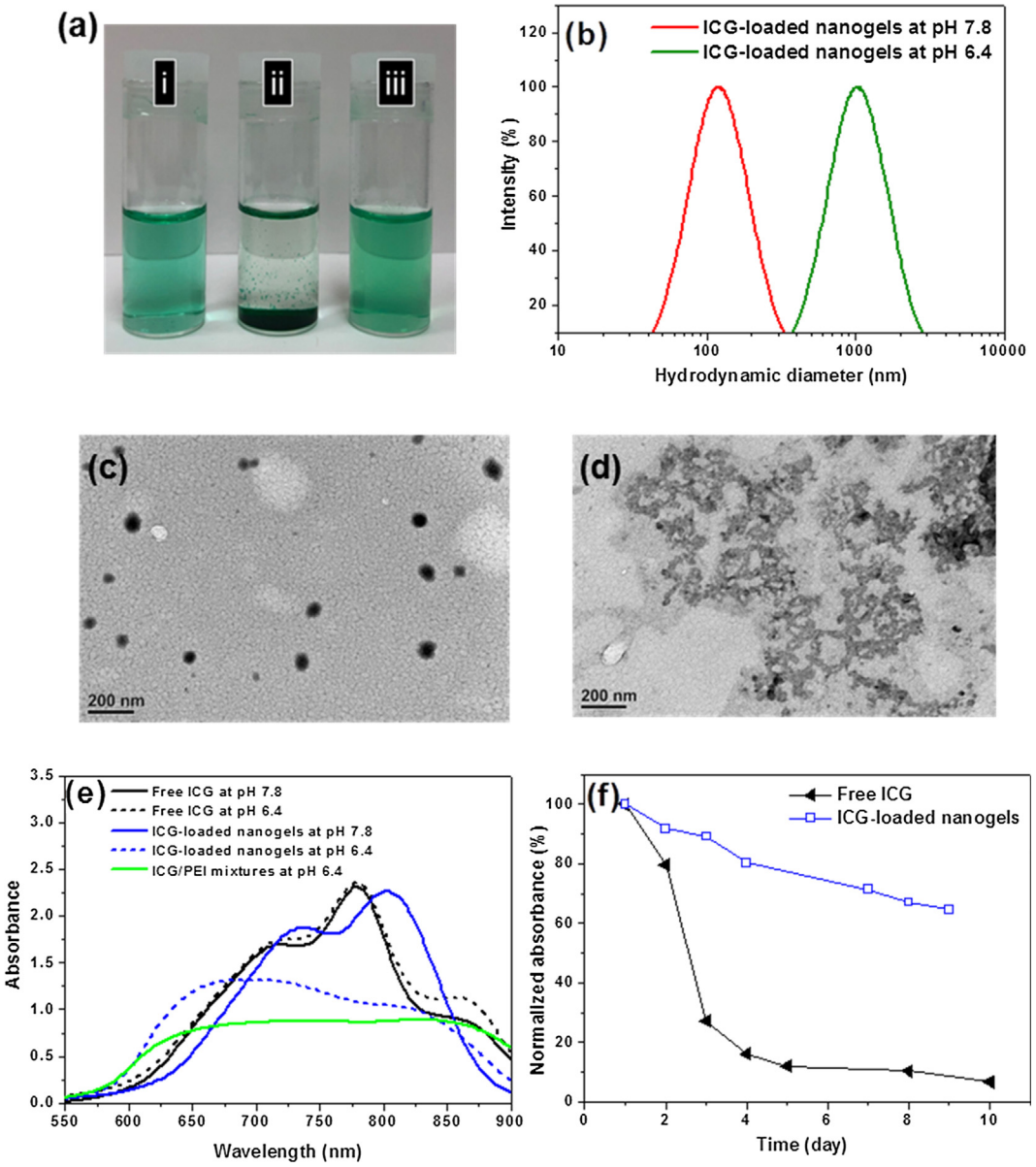

Fig. 7. (a) Photographs of aqueous solutions of (i) free ICG, (ii) ICG/PEI mixtures and (iii) ICG-loaded nanogels. (b) DLS size distribution profiles of ICG-loaded nanogels in aqueous solutions of pH 7.8 and 6.4. TEM images of ICG-loaded nanogels at (c) pH 7.8 and (d) pH 6.4. (e) UV/Vis spectra of free ICG, ICG/PEI mixtures and ICG-loaded nanogels in aqueous solutions. (f) Photostability of free ICG and ICG-loaded nanogels in aqueous solution of pH 7.8 at different time intervals.

the ICG/PEI mixture solution (Fig. 7a), being indicative of the formation of hydrophobic ICG/PEI ionic complexes. Based on this observation, ICG molecules were added to the nanogel solution for preparation of ICG-loaded nanogels. It should be noted that the attained ICG-loaded nanogels were well suspended in the aqueous phase compared to obvious phase separation of the ICG/PEI complexes from the aqueous solution (Fig. 7a). As shown in DLS results (Fig. 7b), the ICG-loaded polymeric nanogels exhibited the particle size (ca. 129 nm) and particle size distribution (PDI 0.24) similar to the pristine nanogels. The findings illustrate that the ICG/PEI ionic complexes could be formed inside the nanogels and effectively stabilized by the outer hydrophilic mPEG segments (Scheme 1). Also, the development of π-π aromatic stacking between the benzoic-imine-rich microdomains and ICG species certainly promotes the stability of ICG/PEI complexes. Consequently, the ICG-loaded nanogels have adequate drug loading efficiency (60.5%) and content (1.7 wt%). Importantly, the DLS data revealed that, as the solution pH being adjusted from 7.8 to 6.4, the particle size of ICG-loaded nanogels was significantly enlarged from 129 nm to 1029 nm and their zeta potential was increased from + 4.9 mV to + 22.6 mV. Moreover, a visible transformation in the morphology of ICG-loaded nanogels from well-dispersed spherical form to irregular-shape aggregates in response to pH reduction was observed by TEM (Fig. 7 c and d). The DLS and TEM characterization clearly indicate that the colloidal structure of ICG-loaded nanogels could be considerably destroyed upon acid-induced disruption of benzoic-imine-based microdomains, thus facilitating the liberation of inner ICG/PEI complexes and their further aggregation in the lack of PEG stabilization effect.

As shown in Fig. 7e, in phosphate buffer (pH 7.8), two characteristic absorption peaks of ICG (20 μM) at ~ 715 nm and 776 nm corresponding to its H-like aggregates and monomers, respectively, were observed, being consistent with the observation by several research groups [41,42]. Notably, as ICG molecules were encapsu-

lated into the polymeric nanogels, the maximum absorption peak of ICG showed a considerable red shift from 776 to 802 nm. This is primarily because the microstructure of ICG was influenced by its binding with PEI segments and association with the hydrophobic microdomains within the nanogels. Such a red shift in the maximum absorption peak of ICG encapsulated within hydrophobic core of various polymeric nanoassemblies was also reported in several literatures [38,43–45]. Interestingly enough, with the pH being adjusted from 7.8 to 6.4, distinct from the nearly unchanged UV/Vis absorption spectra of free ICG solution, an appreciable variation in the UV/Vis absorption spectra of ICG-loaded nanogel solution was observed. In view of the UV/Vis spectrum of amphiphilic ICG in aqueous solution reflecting its aggregation behaviour, [41,42] it was assumed that the aggregation fashion of ICG could be significantly affected by the pH-responsive structural transformation of ICG-encapsulated polymeric nanogels. Here we define $\psi = A_{monomer}/A_{H\text{-like aggregate}}$, where $A_{monomer}$ and $A_{H\text{-like aggregate}}$ are the absorbance of monomer and H-like aggregate of ICG, respectively. The ψ value of ICG-carrying nanogels at pH 7.8 obtained to be ca. 1.21 indicates that most of the added ICG molecules prefer to combine with hydrophobic microdomains as monomers, resulting in reduced amounts of ICG available for H-like aggregates. An appreciable decline in the ψ of ICG-loaded nanogels from 1.21 to 0.77 in response to pH reduction from 7.8 to 6.4 implies that the ICG molecules released from dissociated microdomains are apt to form H-like aggregates by binding to PEI segments. In agreement with the UV/Vis spectrum of ICG-loaded nanogels at pH 6.4, no significant feature absorption peak of ICG monomer was observed in UV/Vis spectrum of ICG/PEI mixtures in aqueous solution (Fig. 7e), evidently proving that the resultant ICG/PEI complexes could assist the formation of H-like ICG aggregates.

Considering that the promoted photostability of ICG in aqueous solution is a prerequisite for potent cancer theranosis, the optical stability of the ICG-loaded nanogels in aqueous phase (pH 7.8) was evaluated by observing the change in absorbance over time. Based on the UV/Vis absorption spectra of free ICG and ICG-loaded nanogels (ICG concentration = 20 μM) (Fig. S5), the maximum absorbance of ICG at each prescribed time is normalized to that at the beginning. Notably, distinct from the remarkable decrease in the normalized absorbance of ICG in aqueous solution over 7 days owing to its self-aggregation and degradation, [35,43,46] the variation in ICG absorbance of ICG-loaded nanogels with time was visibly lower (Fig. 7f), indicating that the encapsulation of ICG within nanogels could sufficiently inhibit self-aggregation and degradation of ICG in the aqueous phase. Besides, the ICG-loaded nanogels in aqueous solution (pH 7.8) remained virtually unchanged particle size during 7 days (Fig. S6). These findings reveal that the ICG-loaded nanogels possessed sound aqueous photo-stability and colloidal stability.

More importantly, as shown in Fig. 8, the ICG release from ICG-loaded nanogels in the aqueous solution (pH 7.8) is remarkably lowered (ca. 8% over 10 h) in comparison with the quick diffusion of free ICG molecules (over 70%) within 10 h through the dialysis membrane in the same medium. This evidently illustrates that the inner ICG/PEI ionic complexes stabilized by the benzoic-imine-rich microdomains can effectively hinder ICG liberation from nanogels. Notably, for ICG-loaded nanogels, the ICG release was largely promoted at pH 6.4 (ca. 65%) compared to at pH 7.8 (ca. 23%) over 24 h. This indicates that the disassembly of ICG-loaded nanogels driven by acid-triggered cleavage of numerous benzoic-imine cross-linkages could effectively promote the release of ICG/PEI complexes from nanogels, thereby further accelerating ICG liberation (Scheme 1). As mentioned by some literatures [47–49], the efficacy of nanoparticulate photodynamic therapy is often compromised by the short life time (<40 ns) and limited diffusion radius (less than 20 nm) of singlet oxygen as well as

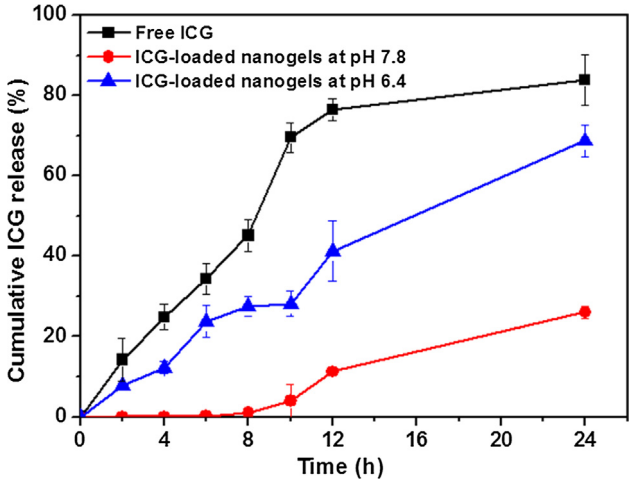

Fig. 8. Cumulative ICG release profiles of ICG-loaded nanogels in aqueous solutions of pH 7.8 and 6.4 at 37 °C. For comparison, diffusion of free ICG across the dialysis membrane in aqueous solution of pH 7.8 is included.

uncontrolled intracellular distribution of photosensitizer. This makes the precise intracellular release of ICG highly desirable. In this work, the developed ICG-loaded nanogels probably achieve intracellular ICG release by acid-activated cargo release, and generate heat and singlet oxygen throughout tumor tissue under NIR irradiation, thus showing great promise in boosting the antitumor efficacy of photodynamic and photothermal therapy. That being said, measurement of release of hydrophobic compounds from colloidal systems by dialysis makes it difficult to infer the true kinetics of release from the material under biological conditions, nevertheless the data indicate that the dye is not irreversibly bound to the gel. Furthermore, a relatively high viability (above 90%) of TRAMP-C1 cells incubated with pristine polymeric nanogels in the concentration range 14–875 μg/mL for 24 h was observed (Fig. S7). This indicates that the polymeric nanogels have essentially no toxicity, thus being suitable for application of drug delivery carriers.

4. Conclusions

To develop the pH-responsive nanogels for effective ICG delivery, the branched PEI-g-mPEG copolymer was synthesized and further covalently cross-linked with hydrophobic TPA molecules upon the formation of acid-labile benzoic-imine bonds. Based on the results of fluorescence and angle-dependent DLS/SLS measurements, the resulting polymeric nanogels have a spherical shape comprising multiple inner benzoic-imine-rich microdomains stabilized by protonated PEI and hydrophilic mPEG segments. Moreover, the addition of more TPA molecules to cross-link PEI-g-mPEG segments enables the formation of more microdomains inside the polymeric nanogels, thus making the colloidal structure more hydrophobic and dense. Taking the advantage of forming ionic complexes with positively-charged PEI segments and π-π stacking with hydrophobic microdomains, the amphiphilic ICG can be effectively encapsulated into the polymeric nanogels. Notably, the ICG-loaded nanogels can considerably enhance the photo-stability of ICG in phosphate buffer and reduce ICG leakage from nanogels. The ICG-loaded nanogels undergoing acid-triggered disassembly due to cleavage of benzoic-imine bonds can appreciably promote ICG release. Although further studies on the in vitro cell uptake and the NIR-induced cytotoxicity and the in vivo biological performance as a drug delivery carrier are essential, the pH-responsive polymeric nanogels show superiority in carrying

ICG molecules and controlling ICG release, thus have great potential for improved ICG delivery.

Declaration of Competing Interest

The authors declare that they have no known competing financial interests or personal relationships that could have appeared to influence the work reported in this paper.

Acknowledgements

This work is supported by the Ministry of Science and Technology, Taiwan (MOST 107-2622-E-005-008 -CC3 and MOST 108-2221-E-005 -024 -MY2).

Appendix A. Supplementary material

Supplementary data to this article can be found online at https://doi.org/10.1016/j.jcis.2019.11.109.

References

[1] P. Wei, G. Gangapurwala, D. Pretzel, M.N. Leiske, L. Wang, S. Hoeppener, S. Schubert, J.C. Brendel, U.S. Schubert, Smart pH-sensitive nanogels for controlled release in an acidic environment, Biomacromolecules 20 (2019) 130–140.
[2] S. Luan, Y. Zhu, X. Wu, Y. Wang, F. Liang, S. Song, Hyaluronic-acid-based pH-sensitive nanogels for tumor-targeted drug delivery, ACS Biomater. Sci. Eng. 3 (2017) 2410–2419.
[3] X. Zhang, K. Achazi, D. Steinhilber, F. Kratz, J. Dernedde, R. Haag, A facile approach for dual-responsive prodrug nanogels based on dendritic polyglycerols with minimal leaching, J. Control. Release 173 (2014) 209–216.
[4] W.H. Chiang, V.T. Ho, W.C. Huang, Y.F. Huang, C.S. Chern, H.C. Chiu, Dual stimuli-responsive polymeric hollow nanogels designed as carriers for intracellular triggered drug release, Langmuir 28 (2012) 15056–15064.
[5] D.Y. Ko, H.J. Moon, B. Jeong, Temperature-sensitive polypeptide nanogels for intracellular delivery of a biomacromolecular drug, J. Mater. Chem. B 3 (2015) 3525–3530.
[6] Y. Liang, K.L. Kiick, Liposome-cross-linked hybrid hydrogels for glutathione-triggered delivery of multiple cargo molecules, Biomacromolecules 17 (2016) 601–614.
[7] D. Maciel, P. Figueira, S. Xiao, D. Hu, X. Shi, J.O. Rodrigues, H. Tomás, Y. Li, Redox-responsive alginate nanogels with enhanced anticancer cytotoxicity, Biomacromolecules 14 (2013) 3140–3146.
[8] T. Nishimura, A. Yamada, K. Umezaki, S. Sawada, S. Mukai, Y. Sasaki, K. Akiyoshi, Self-assembled polypeptide nanogels with enzymatically transformable surface as a small interfering RNA delivery platform, Biomacromolecules 18 (2017) 3913–3923.
[9] S. Hajebi, N. Rabiee, M. Bagherzadeh, S. Ahmadi, M. Rabiee, H. Roghani-Mamaqani, M. Tahriri, L. Tayebi, M.R. Hamblin, Stimulus-responsive polymeric nanogels as smart drug delivery systems, Acta Biomater. 92 (2019) 1–18.
[10] X. Qu, Z. Yang, Benzoic-imine-based physiological-pH-responsive materials for biomedical applications, Chem. Asian J. 11 (2016) 2633–2641.
[11] B.A. Webb, M. Chimenti, M.P. Jacobson, D.L. Barber, Dysregulated pH: a perfect storm for cancer progression, Nat. Rev. Cancer 11 (2011) 671–677.
[12] J.C. Cuggino, M. Molina, S. Wedepohl, C.I.A. Igarzabal, M. Calderón, L.M. Gugliotta, Responsive nanogels for application as smart carriers in endocytic pH-triggered drug delivery systems, Eur. Polym. J. 78 (2016) 14–24.
[13] Y. Li, Q.N. Bui, L.T.M. Duy, H.Y. Yang, D.S. Lee, One-step preparation of pH-responsive polymeric nanogels as intelligent drug delivery systems for tumor therapy, Biomacromolecules 19 (2018) 2062–2070.
[14] K.S. Soni, S.S. Desale, T.K. Bronich, Nanogels: an overview of properties, biomedical applications and obstacles to clinical translation, J. Control. Release 240 (2016) 109–126.
[15] J. Lu, N. Li, Q. Xu, J. Ge, J. Lu, X. Xia, Acetals moiety contained pH-sensitive amphiphilic copolymer self-assembly used for drug carrier, Polymer 51 (2010) 1709–1715.
[16] E.R. Gillies, A.P. Goodwin, J.M.J. Frechet, Acetals as pH sensitive linkages for drug delivery, Bioconjug. Chem. 15 (2004) 1254–1263.
[17] J. Cheng, R. Ji, S.J. Gao, F.S. Du, Z.C. Li, Facile synthesis of acid-labile polymers with pendent ortho esters, Biomacromolecules 13 (2012) 173–179.
[18] R. Tang, W. Ji, D. Panus, R.N. Palumbo, C. Wang, Block copolymer micelles with acid-labile ortho ester side-chains: synthesis, characterization, and enhanced drug delivery to human glioma cells, J. Control. Release 151 (2011) 18–27.
[19] F. Zhan, W. Chen, Z. Wang, W. Lu, R. Cheng, C. Deng, F. Meng, H. Liu, Z. Zhong, Acid-activatable prodrug nanogels for efficient intracellular doxorubicin release, Biomacromolecules 12 (2011) 3612–3620.
[20] S. Li, L. Hu, D. Li, X. Wang, P. Zhang, J. Wang, G. Yan, R. Tang, Carboxymethyl chitosan-based nanogels via acid-labile ortho ester linkages mediated enhanced drug delivery, Int. J. Biol. Macromol. 129 (2019) 477–487.
[21] A. Lia, Y. Wang, T. Chen, W. Zhao, A. Zhang, S. Feng, J. Liu, NIR-laser switched ICG/DOX loaded thermo-responsive polymeric capsule for chemo-photothermal targeted therapy, Eur. Polym. J. 92 (2017) 51–60.
[22] P.R. Jheng, K.Y. Lu, S.H. Yu, F.L. Mi, Free DOX and chitosan-N-arginine conjugate stabilized indocyanine green nanoparticles for combined chemophotothermal therapy, Colloids Surf. B 136 (2015) 402–412.
[23] H. Wang, X. Li, B.W.-C. Tse, H. Yang, C.A. Thorling, Y. Liu, M. Touraud, J.B. Chouane, X. Liu, M.S. Roberts, X. Liang, Indocyanine green-incorporating nanoparticles for cancer theranostics, Theranostics 8 (2018) 1227–1242.
[24] H. Mok, H. Jeong, S.J. Kim, B.H. Chung, Indocyanine green encapsulated nanogels for hyaluronidase activatable and selective near infrared imaging of tumors and lymph nodes, Chem. Commun. 48 (2012) 8628–8630.
[25] J. Gu, W.P. Cheng, J. Liu, S.Y. Lo, D. Smith, X. Qu, Z. Yang, pH-triggered reversible "stealth" polycationic micelles, Biomacromolecules 9 (2008) 255–262.
[26] W.H. Chiang, Y.H. Hsu, F.F. Tang, C.S. Chern, H.C. Chiu, Temperature/pH-induced morphological regulations of shell cross-linked graft copolymer assemblies, Polymer 51 (2010) 6248–6257.
[27] J. Li, X. Meng, J. Deng, D. Lu, X. Zhang, Y. Chen, J. Zhu, A. Fan, D. Ding, D. Kong, Z. Wang, Y. Zhao, Multifunctional micelles dually responsive to hypoxia and singlet oxygen: enhanced photodynamic therapy via interactively triggered photosensitizer delivery, ACS Appl. Mater. Interfaces 10 (2018) 17117–17128.
[28] H. Wen, H. Dong, J. Liu, A. Shen, Y. Li, D. Shi, Redox-mediated dissociation of PEG–polypeptide-based micelles for on-demand release of anticancer drugs, J. Mater. Chem. B 4 (2016) 7859–7869.
[29] A.E. Smith, X. Xu, S.E. Kirkland-York, D.A. Savin, C.L. McCormick, "Schizophrenic" self-assembly of block copolymers synthesized via aqueous RAFT polymerization: from micelles to vesicles, Macromolecules 43 (2010) 1210–1217.
[30] Y.F. Huang, W.H. Chiang, P.L. Tsai, C.S. Chern, H.C. Chiu, Novel hybrid vesicles co-assembled from a cationic lipid and PAAc-g-mPEG with pH-triggered transmembrane channels for controlled drug release, Chem. Commun. 47 (2011) 10978–10980.
[31] W. Schartl (Ed.), Light scattering from polymer solutions and nanoparticle dispersions, Springer-Verlag, Heidelberg, Germany, 2007 [Chapter 4].
[32] E. Kokufuta, K. Ogawa, R. Doi, R. Kikuchi, R.S. Farinato, Geometrical characteristics of polyelectrolyte nanogel particles and their polyelectrolyte complexes studied by dynamic and static light scattering, J. Phys. Chem. B 111 (2007) 8634–8640.
[33] W. Zhang, X. Zhou, H. Li, Y. Fang, G. Zhang, Conformational transition of tethered poly(N-isopropylacrylamide) chains in coronas of micelles and vesicles, conformational transition of tethered poly(N-isopropylacrylamide) chains in coronas of micelles and vesicles, Macromolecules 38 (2005) 909–914.
[34] X. Lu, M. Sun, A.E. Barron, Non-ionic, thermo-responsive DEA/DMA nanogels: synthesis, characterization, and use for DNA separations by microchip electrophoresis, J. Colloid Interface Sci. 357 (2011) 345–353.
[35] Y. Liang, K.L. Kiick, Multifunctional lipid-coated polymer nanogels crosslinked by photo-triggered Michael-type addition, Polym. Chem. 5 (2014) 1728–1736.
[36] M.A. Macchione, C. Guerrero-Beltrán, A.P. Rosso, E.M. Euti, M. Martinelli, M.C. Strumia, M.Á. Muñoz-Fernández, Poly(N-vinylcaprolactam) nanogels with antiviral behavior against HIV-1 infection, Sci. Rep. 9 (2019) 5732.
[37] P. Islam, J.J. Water, A. Bohr, J. Rantanen, Chitosan-based nano-embedded microparticles: impact of nanogel composition on physicochemical properties, Pharmaceutics 9 (2017) 1.
[38] K.T. Hou, T.I. Liu, H.C. Chiu, W.H. Chiang, DOX/ICG-carrying γ-PGA-g-PLGA-based polymeric nanoassemblies for acid triggered rapid DOX release combined with NIR-activated photothermal effect, Eur. Polym. J. 110 (2019) 283–292.
[39] C. Zhang, D. Pan, K. Luo, N. Li, C. Guo, X. Zheng, Z. Gu, Dendrimer-doxorubicin conjugate as enzyme-sensitive and polymeric nanoscale drug delivery vehicle for ovarian cancer therapy, Polym. Chem. 5 (2014) 5227–5235.
[40] K.A. Curtis, D. Miller, P. Millard, S. Basu, F. Horkay, P.L. Chandran, Unusual salt and pH induced changes in polyethylenimine solutions, PLoS ONE 11 (2016) e0158147.
[41] R. Liu, J. Tang, Y. Xu, Y. Zhou, Z. Dai, Nano-sized indocyanine green j-aggregate as a one-component theranostic agent, Nanotheranostics 1 (2017) 430–439.
[42] B. Jung, V.I. Vullev, B. Anvari, Revisiting indocyanine green: effects of serum and physiological temperature on absorption and fluorescence characteristics, IEEE J. Sel. Top. Quant. Electron. 20 (2014) 7000409.
[43] R. Chen, X. Wang, X. Yao, X. Zheng, J. Wang, X. Jiang, Near-IR-triggered photothermal/photodynamic dual-modality therapy system via chitosan hybrid nanospheres, Biomaterials 34 (2013) 8314–8322.
[44] M. Zheng, P. Zhao, Z. Luo, P. Gong, C. Zheng, P. Zhang, C. Yue, D. Gao, Y. Ma, L. Cai, Robust ICG theranostic nanoparticles for folate targeted cancer imaging an highly effective photothermal therapy, ACS Appl. Mater. Interfaces. 6 (2014) 6709–6716.
[45] L. Yu, A. Dong, R. Guo, M. Yang, L. Deng, J. Zhang, DOX/ICG coencapsulated liposome-coated thermosensitive nanogels for NIR-triggered simultaneous drug release and photothermal effect, ACS Biomater. Sci. Eng. 4 (2018) 2424–2434.
[46] Z. Wan, H. Mao, M. Guo, Y. Li, A. Zhu, H. Yang, H. He, J. Shen, L. Zhou, Z. Jiang, C. Ge, X. Chen, X. Yang, G. Liu, H. Chen, Highly efficient hierarchical micelles

integrating photothermal therapy and singlet oxygen-synergized chemotherapy for cancer eradication, Theranostics 4 (2014) 399–411.
[47] X. Zhang, Q. Yan, D.N. Mulatihan, J. Zhu, A. Fan, Z. Wang, Y. Zhao, Pharmaceutical micelles featured with singlet oxygen-responsive cargo release and mitochondrial targeting for enhanced photodynamic therapy, Nanotechnology 29 (2018) 255101.
[48] C. Feng, D. Zhu, L. Chen, Y. Lu, J. Liu, N.Y. Kim, S. Liang, X. Zhang, Y. Lin, Y. Ma, C. Dong, Targeted delivery of chlorin e6 via redox sensitive diselenide-containing micelles for improved photodynamic therapy in cluster of differentiation 44-overexpressing breast cancer, Front Pharmacol. 10 (2019) 369.
[49] X. Li, M. Gao, K. Xin, L. Zhang, D. Ding, D. Kong, Z. Wang, Y. Shi, F. Kiessling, T. Lammers, J. Cheng, Y. Zhao, Singlet oxygen-responsive micelles for enhanced photodynamic therapy, J. Control. Release 260 (2017) 12–21.